Analysis of resonance and anti-resonance frequencies in a wireless power transfer system: analytical model and experiments

Binh Duc Truong, Caleb Roundy, Erik Andersen and Shad Roundy

***Abstract*—This letter presents a magnetic coupling wireless power transfer system (WPTS) configured in a series-series topology and operating at both resonance and anti-resonance frequencies which occur due to the parasitic coil capacitances. It is shown that their effects on system dynamics cannot be ignored. A mathematical model based on circuit theory is developed and the analytical solution for the power transferred to an electrical load is derived. A technique for extracting coil parameters such as resistance, inductance and capacitance from impedance measurements is proposed. The complete model is first experimentally verified and then used for further numerical investigations.**

***Index Terms*—Wireless Power Transfer, (Anti-)Resonance Frequencies.**

I. INTRODUCTION

WIRELESS power transfer systems utilizing magnetically coupled coils has gained more and more research interest due to its wide range of applications such as electric vehicles [1], wireless sensor networks [2], and implantable biomedical devices [3], [4]. Although the WPT concept has been explored at the beginning of the 20th century by Nikola Tesla [5], the recent work by a group at MIT [6] has led to a massive increase in research and commercial activity. In particular, the MIT group proposed an improved inductive power transfer system based on magnetic resonance coupling using a four-coil system which allows a more efficient operation over a farther distance range than similar previous methods [6]. This long distance operation has opened up many applications for charging electronic devices without annoying wires.

Different system architectures with three or four coils were widely reported [6], [7]. However, recently Seo *et. al.* revealed that three/four-coil systems do not necessarily perform better than two-coil type [8], without denying that the former could offer more degrees of freedom for optimization. In some particular circumstances when the device sizes are strictly constrained (e.g., an artificial cardiac pacemaker), the simplicity of the two-coil structure is more appropriate. It is therefore the objective of this paper. In a two-coil WPTS, depending on how the capacitors are connected to the coils, there are four basic compensation topologies, which are series-series (SS), series-parallel (SP), parallel-parallel (PP) and parallel-series (PS) [9], [10]. When investigating their operation, the authors neglected the parasitic capacitance of the coil. However, we observe from experiments that for the SS topology the anti-resonant frequency caused by the parasitic capacitance in parallel with the coil inductance is close to the resonant frequency when such a parasitic capacitance is in the same range as the added capacitance. In this case, the impact of parasitic capacitance is considerable and the dynamic behavior of the system is thus of great interest to comprehensively analyze.

Coupled mode theory (CMT) addresses the clear physics of the power transfer process [6], however, most electrical researchers are more familiar with the circuit theory (CT) approach. Here we choose the CT as a means to study the WPTS given the fact that both methods are different but equivalent tools to describe the same phenomenon, meaning that the same conclusions are obtained regardless of approach [11], [12]. An advantage of the CT is to offer an explicit expression of the power delivered to a load, providing an efficient technique to design and optimize the system performance. In this work, a compact analytical model is presented and validated by experiments, which is the premise for further analysis. Note that, we focus on power optimization issues in low-power systems rather than maximizing transmission efficiency.

II. THEORETICAL MODELING

Figure 1 shows the complete model of the two-coil WPT system configured in series-series topology, in which the parasitic capacitances of both transmitter and receiver coils (i.e., C_{p1} and C_{p2} respectively) are taken into account. The load coil L_2 is connected to a fixed capacitor C_2 and a resistor R_{L} in series. The load stray capacitance C_{pL} is included for a general model, which is typically neglected in the literature. The drive coil L_1 is excited by a power source V_{S} with output impedance R_{S}. A variable capacitor C_1 is utilized

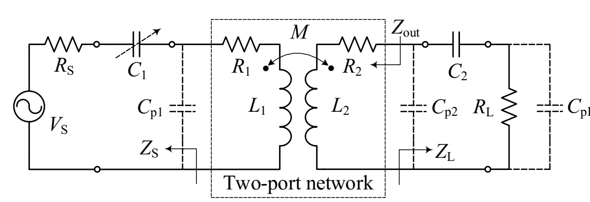

Fig. 1: Complete circuit model of the two-coil WPT system.

B. D. Truong, E. Andersen and S. Roundy were with the Department of Mechanical Engineering, C. Roundy was with the Department of Biology Engineering, University of Utah, Salt Lake, UT, 84112 USA, e-mail: Binh.D.Truong@utah.edu and Shad.Roundy@utah.edu.

This work was supported by the National Science Foundation ASSIST Nanosystems ERC under Award Number EEC-1160483.

Manuscript submitted MONTH DAY, 2018.

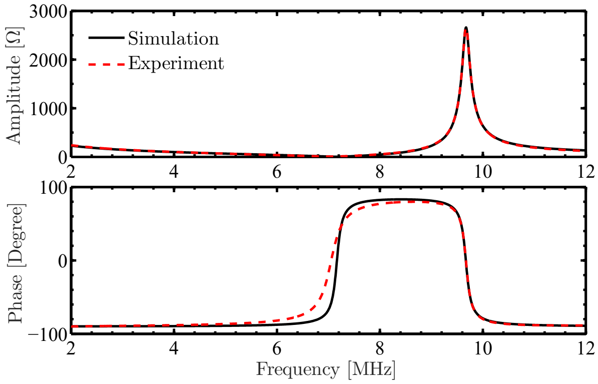

Fig. 2: Impedance amplitude and phase of the transmitter coil.

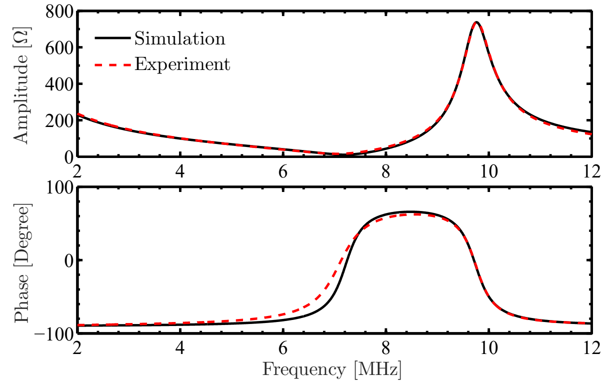

Fig. 3: Impedance amplitude and phase of the receiver coil.

for resonance frequency matching. The magnetic interaction between the two coils is modeled as a mutual inductance $M = k\sqrt{L_1 L_2}$ where $0 \leq k \leq 1$ is the coupling coefficient. R_1 and R_2 represents the parasitic resistances of L_1 and L_2 correspondingly. In practice, (R_1, L_1, C_{p1}) or (R_2, L_2, C_{p2}) are inseparable. However, in order to reduce the complexity of analytical computation without compromising the generality of the problem, we conventionally define that the two-port network is formed only by (R_1, L_1) and (R_2, L_2) while the source impedance Z_s now includes both C_1 and C_{p1}, and the load impedance Z_L consists of C_2, C_{p2}, R_L and C_{pL}.

The expressions of these impedances, and the Z-parameters (i.e., the impedance matrix [13]) of the two-port network are

$$Z_{11} = R_1 + j\omega L_1, \tag{1}$$

$$Z_{22} = R_2 + j\omega L_2, \tag{2}$$

$$Z_{12} = Z_{21} = j\omega M, \tag{3}$$

$$Z_S = \left[j\omega C_{p1} + \left(R_S + \frac{1}{j\omega C_1} \right)^{-1} \right]^{-1}, \tag{4}$$

$$Z_L = \left[j\omega C_{p2} + \left(\frac{1}{j\omega C_2} + \left(j\omega C_{pL} + \frac{1}{R_L} \right)^{-1} \right)^{-1} \right]^{-1} \tag{5}$$

where ω is the driving angular frequency.

The power transferred to the load is then derived as follows

$$P_L = \frac{1}{2} |V_{th}|^2 \frac{|Z_{21}|^2 \Re\{Z_L\}}{\left| (Z_{11} + Z_S)(Z_{out} + Z_L) \right|^2} \tag{6}$$

$$\text{where } V_{th} = V_S \frac{\dfrac{1}{j\omega C_{p1}}}{\dfrac{1}{j\omega C_{p1}} + \dfrac{1}{j\omega C_1} + R_S} \tag{7}$$

$$\text{and } Z_{out} = Z_{22} - \frac{Z_{12} Z_{21}}{Z_{11} + Z_S}. \tag{8}$$

Here Z_{out} is the output impedance and V_{th} is the Thévenin equivalent voltage in series with Z_S (not shown in the Figure). The proposed mathematical technique can also be generalized and applied to obtain the closed-form of P_L for any similar structure or configuration, in which Z_S, Z_L and V_S are modified accordingly.

III. Experimental validation

A. System parameter identification

In this section, we propose a numerical optimization scheme for identifying the electrical properties of each coil, which has been already connected to an external capacitor. In order to avoid any possible dynamic interferences between the two coils, we measure their impedances separately without integrating them on the complete experimental setup. Here, we denote R, L, C_p and C for both of transmitter and receiver coils since their models are identical.

The complex impedance of the coil, Z_c, and its amplitude $|Z_c|$ and phase ϕ are expressed as

$$Z_c = \frac{1}{j\omega C} + \frac{\dfrac{1}{j\omega C_p}(j\omega L + R)}{\dfrac{1}{j\omega C_p} + j\omega L + R}, \tag{9}$$

$$|Z_c| = \left(\Re\{Z_c\}^2 + \Im\{Z_c\}^2 \right)^{1/2}, \tag{10}$$

$$\phi = \tan^{-1} \frac{\Im\{Z_c\}}{\Re\{Z_c\}} \tag{11}$$

$$\text{where } \Re\{Z_c\} = \frac{R}{(\omega^2 L C_p - 1)^2 + (\omega R C_p)^2}, \tag{12}$$

$$\Im\{Z_c\} = -\frac{1}{\omega C} - \frac{\omega(\omega^2 L^2 C_p + R^2 C_p - L)}{(\omega^2 L C_p - 1)^2 + (\omega R C_p)^2}. \tag{13}$$

$|Z_c|$ and ϕ are measured by a network analyzer. It should be noted that the compensation capacitance C_2 is fixed at a chosen value while C_1 is tuned so that both coils have the same resonant frequency (i.e., at which the impedance amplitude is minimum). In contrast, the anti-resonant frequency (i.e., at which the impedance amplitude is maximum) depends on the parasitic capacitance, and therefore, is uncontrollable in such a circumstance.

The parametric identification problem is formulated as follows

$$\min_{R,L,C_p,C} \sum_{i=1}^{n} \left({}^{e}|Z_c| - {}^{s}|Z_c| \right)^2 \tag{14}$$

where n is the number of experimental samples collected, ${}^{e}|Z_c|$ and ${}^{s}|Z_c|$ are experimental and simulated data respectively. To solve this nonlinear optimization problem with constraints placed on the value of the variables (i.e., all of them are positive), the nonlinear Interior Point (IP) or Sequential Quadratic Programming (SQP) methods are utilized [14]. Due to the fact that the resonance/anti-resonance frequencies are likely to result from various combinations of the inductance and capacitance, we not only consider the coil impedance around the resonance/anti-resonance frequencies but also account for

This article has been accepted for publication in a future issue of this journal, but has not been fully edited. Content may change prior to final publication. Citation information: DOI 10.1109/TCSII.2018.2878662, IEEE Transactions on Circuits and Systems II: Express Briefs

TABLE I: Coil Parameters. Notation: f_0 - resonant frequency, f_1 - anti-resonant frequency, superscript: T - Transmitter, R - Receiver

Transmitter		**Receiver**	
C_1, pF	334.32	C_2, pF	333.82
C_{p1}, pF	406.25	C_{p2}, pF	407.08
L_1, μH	0.667	L_2, μH	0.692
R_1, Ω	0.62	R_2, Ω	2.20
${}^{\mathrm{T}}f_0$, MHz	7.037	${}^{\mathrm{R}}f_0$, MHz	7.056
${}^{\mathrm{T}}f_1$, MHz	9.675	${}^{\mathrm{R}}f_1$, MHz	9.762

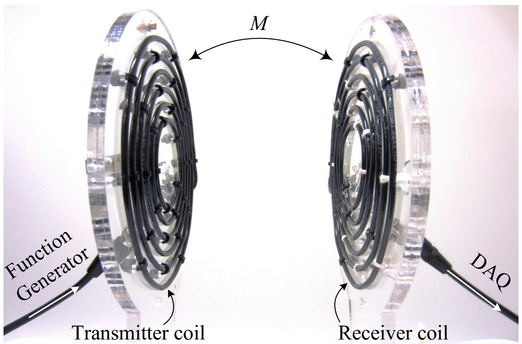

Fig. 4: Experiment setup.

a wide range of frequency. This consideration is expected to provide a unique solution to the two coil parameters. In order to test the accuracy of the method, we first use LT-SPICE simulation as a source of data with known parameters. Hence, these simulations play the role that measurements would do in a real experimental characterization. Comparison of "true" and estimated values shows that the approach can accurately recover the specified model parameters.

Figure 2 and 3 show a good agreement between results based on measured and estimated parameters for both drive and load coils, with a slight difference in phases only. The measurements are conducted from 2 MHz to 12 MHz where the maximum number of samples provided by the network analyzer is $n = 1601$. Note that, while the two coils exhibit the resonant and anti-resonant frequencies close to those of each other, their highest impedance amplitudes are recognizably different even when they are supposed to be identical in design. To be specific, $\max|Z_c| = 2.65\,\mathrm{k}\Omega$ for the transmitter coil and $\max|Z_c| = 738.36\,\Omega$ for the receiver coil. This can be explained by the difference between R_1 and R_2 due to errors during soldering and/or the property of two added capacitors (C_2 might have higher series resistance than C_1 does). However, this difference does not influence the general dynamics of the system, despite of the fact that it may slightly reduce the power delivered to the load. In addition, the resonance/anti-resonances of the WPTS can be approximately obtained by setting $\phi = 0$, or in other words $\Im\{Z_c\} = 0$. The two analytical solutions are presented in Appendix A. All the extracted parameters are listed in Table I, which will be used for all following simulations.

B. Measurement results

Figure 4 depicts the transmit and receive coil setup, where a function generator is utilized as the source power to drive

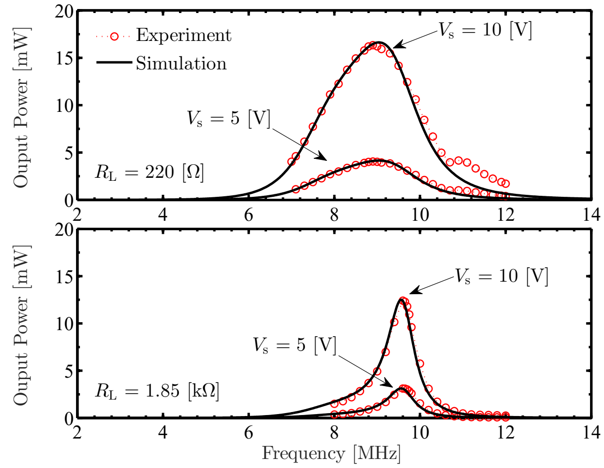

Fig. 5: Frequency responses with two different loads R_L and two source voltage V_S.

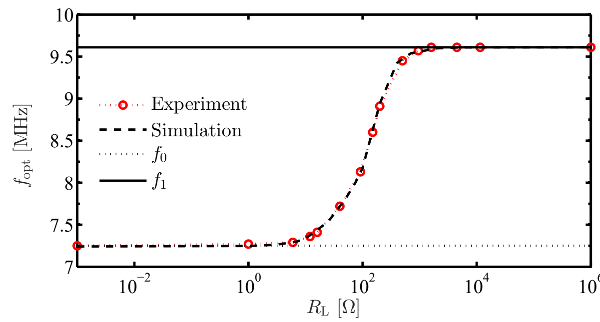

Fig. 6: Optimal frequency f_{opt} with respect to the electrical load R_L.

the transmitter coil and the voltage induced in the load V_L is captured by an oscilloscope. For the sinusoidal input signals, the average delivered power is calculated as $P_L = \frac{1}{2}\frac{|V_L|^2}{R_L}$. The output impedance of the source is set as $R_S = 50\,\Omega$. The stray capacitance of the load resistor is measured equal to $C_{pL} \approx$ 15.5 pF, which can be changed from one to another resistor, however, the difference is typically small and negligible. The distance between the two coils is about 10 cm. The coupling factor is determined by fitting the model simulations to the experimental data at $V_S = 5$ V and $R_L = 220\,\Omega$, which results in $k = 57.19 \times 10^{-3}$. The squared magnetic coupling factor k^2 is often used to characterize the coupling since it is proportional to the transmission efficiency [15]. The value $k^2 = 2.7 \times 10^{-3}$ is then kept constant while verifying other cases.

Figure 5 shows a good agreement between the model predictions obtained from (6) and the measurement results, with different loads and input voltages. Since the system is operating at high frequencies, we choose to evaluate the steady-state performances with discrete frequencies instead of using frequency-swept signals. We also observe that the output power could drop down to $\sim 80\,\%$ in comparison with that of steady state due to the effect of sweep rate. As can be seen in the same Figure, the optimal frequency f_{opt} changes with respect to the electrical load, in particular, $f_{opt} = 8.9$ MHz for $R_L = 220\,\Omega$ and $f_{opt} = 9.6$ MHz for $R_L = 1.85\,\mathrm{k}\Omega$.

For a further investigation, we vary the resistance and

This article has been accepted for publication in a future issue of this journal, but has not been fully edited. Content may change prior to final publication. Citation information: DOI 10.1109/TCSII.2018.2878662, IEEE Transactions on Circuits and Systems II: Express Briefs

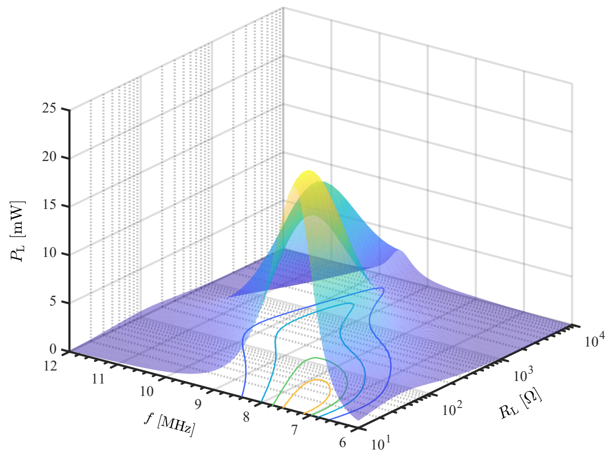

Fig. 7: Simulation results of the output power P_L as a function of the drive frequency f and the load resistance R_L in the weak coupling regime $k^2 = 2.7 \times 10^{-3}$.

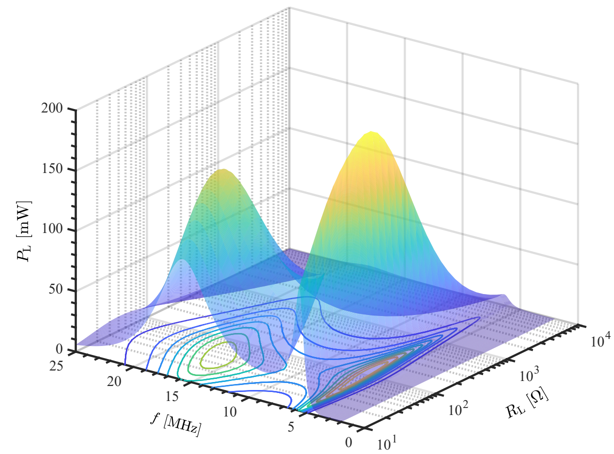

Fig. 8: Simulation results of the output power P_L as a function of the drive frequency f and the load resistance R_L in the strong coupling regime $k^2 = 0.565$.

find its corresponding optimal frequency by examining the maximum voltage across the load. The obtained results are presented in Figure 6, showing that $f_{opt} \in [f_0, f_1]$ and f_{opt} increases with the load resistance. This particular property is present for all series-series WPTS, where the parasitic capacitance cannot be neglected, under the effects of the resonance and anti-resonance frequencies. This is the first time the phenomenon is reported in the field of WPT and it opens more options to optimize the transferred power depending on the loading conditions. Here, $f_0 = 7.25$ MHz and $f_1 = 9.61$ MHz, which are slightly different from ${}^{T/R}f_0$ and ${}^{T/R}f_1$ of each single coil reported in Table I.

IV. Discussion

As demonstrated by the previous sections, the complete model based on the circuit theory formalism has captured the main physics of the complex WPTS well. It is, therefore, of great interest to utilize the model (i.e., mainly based on formula (6)) to further analyze other characteristics and to reveal a comprehensive physical insight of the system.

Figure 7 gives a more thorough picture of Figures 5 and 6, showing the variation of the output power as a function of the drive frequency and the load resistance with the same squared coupling factor $k^2 = 2.7 \times 10^{-3}$ and the input source voltage $V_S = 10$ V. The maximum power of 22.87 mW is achieved at $R_L = 12.2\,\Omega$ when $f = f_0$. For $f = f_1$, the maximum power is 13.88 mW at $R_L = 605.0\,\Omega$ approximately. Defining the transducer efficiency (i.e., transducer power gain) as a ratio of the power delivered to the load P_L to the power available from the source $P_{avs} = \frac{1}{8}\frac{|V_S|^2}{R_S}$, $\eta = \frac{P_L}{P_{avs}}$, the maximum efficiency achievable at this coupling coefficient is $\sim 9.15\,\%$ where $P_{avs} = 250$ mW. Note, that P_{avs} is not the power actually taken from the source, the maximum power available at a given source voltage and resistance. P_{avs} is independent of the input impedance of the network [13], therefore it is much more convenient to compute the actual transferred power from known P_{avs} and η without determining the power input to the network.

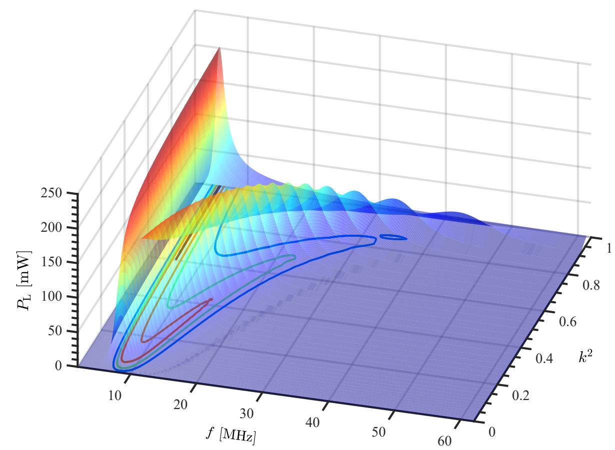

Fig. 9: Simulation results of the output power P_L as a function of the drive frequency f and the coupling factor k^2.

The simulation results in Figure 8 are created using a higher squared coupling factor $k^2 = 0.565$ while keeping the same input voltage $V_S = 10$ V. It is revealed that the optimal frequency for each load is now no longer constrained by the resonant and anti-resonant frequencies. Instead, f_{opt} is dominantly affected by the frequency splitting phenomenon in the strong coupling regime that is well-known for four-coil systems [7]. For instance, the two extreme frequencies of $R_L = 110\ \Omega$ are $f_l = 6.21$ MHz and $f_h = 17.51$ MHz which give $P_{L-l} = 199.68$ mW and $P_{L-h} = 132.34$ mW respectively. Although the maximum output power at f_h is $\sim 33.72\,\%$ lower than that at f_l, the bandwidth around f_h is about ~ 3.15 times larger (i.e., $B_{f_h} = 7.63$ MHz in comparison with $B_{f_l} = 2.42$ MHz) as can be seen in the contour plot of Figure 8. The maximum achieved transducer efficiency at this coupling factor is 79.9 % with P_{L-l}.

The impact of the strong coupling on the system dynamics is depicted in Figure 9 with a fixed load of $R_L = 110\,\Omega$ and $V_S = 10$ V. The critical coupling factor at which the frequency splitting phenomena start occurring is $k_{cr}^2 \approx 0.1$. Unlike what has been described in [7], among others, the maximum

This article has been accepted for publication in a future issue of this journal, but has not been fully edited. Content may change prior to final publication. Citation information: DOI 10.1109/TCSII.2018.2878662, IEEE Transactions on Circuits and Systems II: Express Briefs

output powers on the two extreme frequency branches are very asymmetric. The power on the high frequency branch drops significantly compared to that on the lower frequency branch as k^2 increases. In order to comprehend the reason behind this behavior, we theoretically compare three models: (i) Complete model presented in Section II, (ii) A model of a typical series-series configuration where the parasitic capacitance in parallel with the coil is eliminated, and (iii) A model only takes the parasitic capacitances into account while added capacitors are removed. The simulation results show that the investigated phenomenon only occurs when the parasitic capacitances are presence, corresponding to cases (i) and (iii). For $f = f_1$ and $k^2_{\mathrm{cr}} \leq k^2 \leq 0.6$, the efficiency gradually rises from more than 70 % to 80 % and then remains almost unchanged for higher k^2. By contrast, in the weak coupling regime, $k^2 \leq k^2_{\mathrm{cr}}$, the maximum power to the load decreases dramatically. We found that applying the impedance matching approach to the source/load is a potential solution to overcome this challenge. However, performance of a system with and without impedance matching networks is very different. It is out of scope of this paper and is open for future analysis.

V. Concluding remarks

We presented a theoretical study and experimental validation of a WPTS taking into consideration the resonance and anti-resonance frequencies of both the transmitter and receiver. That analysis led to an investigation of the optimal choice of drive frequency in the weak coupling regime, which depends on the electrical load. A closed-form analytical model developed based on the circuit theory was shown to be in good agreement with the measured data. The complete model was utilized as a means to thoroughly analyze the system dynamics. The numerical results showed that the efficiency of the WPTS under consideration could reach a high level without any optimization techniques in the strong coupling regime. While most of authors have considered a fixed load resistance (typically choose $R_{\mathrm{L}} = R_{\mathrm{S}} = 50\,\Omega$), we offered another perspective when analyzing the system behavior in more general cases with load, frequency and coupling factor varying. It should be noted that the resonance and anti-resonance operation is completely different from the frequency splitting behavior reported in the literature. The former is dominant at low coupling coefficient and only occurs in presence of coil parasitic capacitances. In contrast, the latter was only observed in the high coupling regime regardless of whether those parasitic capacitances are present or not. Furthermore, in situations where parasitic capacitances are significant, they cause the asymmetric property of the frequency splitting phenomenon. These important findings have not been reported anywhere else.

Appendix
Analytical solution of the resonance and anti-resonance frequencies

The resonance and anti-resonance are determined by the equation

$$-\frac{1}{\omega C} - \frac{\omega(\omega^2 L^2 C_{\mathrm{p}} + R^2 C_{\mathrm{p}} - L)}{(\omega^2 L C_{\mathrm{p}} - 1)^2 + (\omega R C_{\mathrm{p}})^2} = 0, \quad (15)$$

which results in

$$f_0 = \frac{1}{2\pi}\left[\frac{C/2 + C_{\mathrm{p}}}{LC_{\mathrm{p}}(C + C_{\mathrm{p}})} - 2\left(\frac{R}{L}\right)^2 - \frac{1}{2}\frac{\sqrt{\sigma}}{L^2 C_{\mathrm{p}}(C + C_{\mathrm{p}})}\right]^{1/2}, \quad (16)$$

$$f_1 = \frac{1}{2\pi}\left[\frac{C/2 + C_{\mathrm{p}}}{LC_{\mathrm{p}}(C + C_{\mathrm{p}})} - 2\left(\frac{R}{L}\right)^2 + \frac{1}{2}\frac{\sqrt{\sigma}}{L^2 C_{\mathrm{p}}(C + C_{\mathrm{p}})}\right]^{1/2} \quad (17)$$

$$\text{where } \sigma = \left[R^2 C_{\mathrm{p}}(C + C_{\mathrm{p}}) - LC\right]^2 - 4L(RC_{\mathrm{p}})^2(C + C_{\mathrm{p}}). \quad (18)$$

For instance, substituting C_1, C_{p1}, L_1 and R_1 of the transmitter coil in Table I into (16) and (17), we get ${}^{\mathrm{T}}f_0 = 7.163$ MHz and ${}^{\mathrm{T}}f_1 = 9.666$ MHz. The difference between these analytical solutions and the measured results is less than 1.8 %. A similar observation is obtained for the receiver coil.

In the case where the parasitic capacitance is negligibly small $C_{\mathrm{p}} \approx 0$, (15) reduces to $1/(\omega C) + \omega L = 0$. Therefore there only exists the well-known resonance frequency of the series-series configuration $f^* = 1/(2\pi\sqrt{LC})$. The closed-form of f_0 and f_1 is much more complicated than that of f^* due to the presence of C_{p}.

References

[1] S. Y. Choi, B. W. Gu, S. Y. Jeong, and C. T. Rim, "Advances in wireless power transfer systems for roadway-powered electric vehicles," *IEEE Journal of Emerging and Selected Topics in Power Electronics*, vol. 3, pp. 18–36, March 2015.

[2] L. Xie, Y. Shi, Y. T. Hou, and H. D. Sherali, "Making sensor networks immortal: An energy-renewal approach with wireless power transfer," *IEEE/ACM Transactions on Networking*, vol. 20, pp. 1748–1761, Dec 2012.

[3] X. Li, Y. Li, C. Tsui, and W. Ki, "Wireless power transfer system with $\sigma\delta$-modulated transmission power and fast load response for implantable medical devices," *IEEE Transactions on Circuits and Systems II: Express Briefs*, vol. 64, pp. 279–283, March 2017.

[4] E. Y. Chow, C. L. Yang, Y. Ouyang, A. L. Chlebowski, P. P. Irazoqui, and W. J. Chappell, "Wireless powering and the study of rf propagation through ocular tissue for development of implantable sensors," *IEEE Transactions on Antennas and Propagation*, vol. 59, pp. 2379–2387, June 2011.

[5] N. Tesla, "Apparatus for transmitting electrical energy," *US Patent*, May 1907.

[6] A. Kurs, A. Karalis, R. Moffatt, J. D. Joannopoulos, P. Fisher, and M. Soljačić, "Wireless power transfer via strongly coupled magnetic resonances," *Science*, vol. 317, no. 5834, pp. 83–86, 2007.

[7] A. P. Sample, D. T. Meyer, and J. R. Smith, "Analysis, experimental results, and range adaptation of magnetically coupled resonators for wireless power transfer," *IEEE Transactions on Industrial Electronics*, vol. 58, pp. 544–554, Feb 2011.

[8] S. Dong-Wook, L. Jae-Ho, and L. H. Soo, "Study on two-coil and four-coil wireless power transfer systems using Z-parameter approach," *ETRI Journal*, vol. 38, no. 3, pp. 568–578, 2016.

[9] S. Li and C. C. Mi, "Wireless power transfer for electric vehicle applications," *IEEE Journal of Emerging and Selected Topics in Power Electronics*, vol. 3, pp. 4–17, March 2015.

[10] C. M. de Miranda and S. F. Pichorim, "A self-resonant two-coil wireless power transfer system using open bifilar coils," *IEEE Transactions on Circuits and Systems II: Express Briefs*, vol. 64, pp. 615–619, June 2017.

[11] M. Kiani and M. Ghovanloo, "The circuit theory behind coupled-mode magnetic resonance-based wireless power transmission," *IEEE Transactions on Circuits and Systems I: Regular Papers*, vol. 59, pp. 2065–2074, Sept 2012.

[12] D. S. Ricketts, M. J. Chabalko, and A. Hillenius, "Experimental demonstration of the equivalence of inductive and strongly coupled magnetic resonance wireless power transfer," *Applied Physics Letters*, vol. 102, no. 5, p. 053904, 2013.

[13] S. J. Orfanidis, *Electromagnetic Waves and Antennas*. ECE Department, Rutgers University, Online ed., 2016.

[14] S. W. Jorge Nocedal, *Numerical Optimization*. Springer series in operations research, Springer, 2nd ed ed., 2006.

[15] S. Assawaworrarit, X. Yu, and S. Fan, "Robust wireless power transfer using a nonlinear parity-time-symmetric circuit," *Nature*, vol. 546, 6 2017.